



# **ESTCP MUNITIONS RESPONSE LIVE SITE DEMONSTRATION at Former Camp Beale, CA**

---



**LBNL Hand-Held UXO Discriminator  
MR-201166**

**Demonstration Report**

**April 2012**

p.o.c. Erika Gasperikova, [egasperikova@lbl.gov](mailto:egasperikova@lbl.gov), 510-486-4930

## **DISCLAIMER**

This document was prepared as an account of work sponsored by the United States Government. While this document is believed to contain correct information, neither the United States Government nor any agency thereof, nor The Regents of the University of California, nor any of their employees, makes any warranty, express or implied, or assumes any legal responsibility for the accuracy, completeness, or usefulness of any information, apparatus, product, or process disclosed, or represents that its use would not infringe privately owned rights. Reference herein to any specific commercial product, process, or service by its trade name, trademark, manufacturer, or otherwise, does not necessarily constitute or imply its endorsement, recommendation, or favoring by the United States Government or any agency thereof, or The Regents of the University of California. The views and opinions of authors expressed herein do not necessarily state or reflect those of the United States Government or any agency thereof or The Regents of the University of California.

Ernest Orlando Lawrence Berkeley National Laboratory is an equal opportunity employer.

# **Cued survey with a hand-held UXO discriminator at Camp Beale, CA**

Erika Gasperikova<sup>1</sup>, Vamsi Vytla<sup>1</sup>, Todd Jobe<sup>2</sup>, Levi Kennedy<sup>2</sup>, and Xianyang Zhu<sup>2</sup>

<sup>1</sup>Lawrence Berkeley National Laboratory, One Cyclotron Road, MS:90R1116, Berkeley, CA 94720

<sup>2</sup>Signal Innovations Group, Inc., 4721 Emperor Blvd., Suite 330, Durham, NC 27703

## OVERVIEW

---

The LBNL group has developed a prototype of a hand-held UXO discriminator (14-in = 0.35 m cube) that is able to discriminate small (20 mm) UXO objects at a depth of 0.45 m and large (105 and 155 mm) UXO objects at the depth of 0.85 m from harmless scrap metal. This hand-held prototype incorporates the key features of the cart-mounted system: three orthogonal transmitters and ten pairs of receivers, and difference or gradient measurements that significantly reduce the ambient and motion noise, and greatly enhance the sensitivity to the gradients of the target. The system characterizes the target from a single position. A demonstration survey at a standard test site showed that the same discrimination capabilities afforded by the cart-mounted system are available in the hand-held unit, although with a slightly reduced depth of detection. To demonstrate the system performance at a live site, LBNL participated in the ESTCP UXO discrimination study at the former Camp Beale, Marysville, CA where the hand-held UXO discriminator was operated in the cued mode. The system was brought to marked locations (flags) and ran in the characterization/discrimination mode. The system had no positioning capability; hence data around the flag were acquired using a three or five-point template with the system oriented in a single direction. The survey took two weeks, and we occupied 900 flag locations within 18 grids selected by the program office. UXO and scrap discrimination and priority dig list were be done by Signal Innovations Group, Inc.

## TABLE OF CONTENT

<b>1. INTRODUCTION</b> .....	<b>5</b>
<b>2. TECHNOLOGY DESCRIPTION</b> .....	<b>7</b>
<b>3. DEMONSTRATION SURVEY</b> .....	<b>12</b>
<b>4. DATA ANALYSIS AND INTERPRETATION</b> .....	<b>14</b>
<b>4.1 DATA PROCESSING</b> .....	<b>14</b>
<b>4.2 DISCRIMINATION USING THE ISOLATE PROCESS</b> .....	<b>14</b>
4.2.1 <i>Feature Selection with BNet</i> .....	16
4.2.2 <i>Semi-Supervised Learning Classifier</i> .....	17
4.2.3 <i>Batch-mode Active Learning (AL)</i> .....	18
4.2.4 <i>SIG Isolate Process Overview</i> .....	19
4.2.5 <i>Application to Camp Beale Data</i> .....	21
4.2.6 <i>Retrospective Analysis</i> .....	25
<b>4.3 DISCRIMINATION USING TEMPLATE-MATCH APPROACH</b> .....	<b>29</b>
4.3.1 <i>Data Analysis</i> .....	29
4.3.2 <i>Retrospective Analysis</i> .....	31
<b>5. PERFORMANCE ASSESSMENT</b> .....	<b>33</b>
5.1 <i>Statistical Approach Performance</i> .....	33
5.2 <i>Template-match Approach Performance</i> .....	35
<b>6. CONCLUSIONS</b> .....	<b>36</b>
<b>7. ACKNOWLEDGMENTS</b> .....	<b>36</b>
<b>8. REFERENCES</b> .....	<b>37</b>
<b>9. ACRONYMS</b> .....	<b>39</b>

## 1. INTRODUCTION

In 2003, the Defense Science Board observed: “The ... problem is that instruments that can detect the buried UXOs also detect numerous scrap metal objects and other artifacts, which leads to an enormous amount of expensive digging. Typically 100 holes may be dug before a real UXO is unearthed! The Task Force assessment is that much of this wasteful digging can be eliminated by the use of more advanced technology instruments that exploit modern digital processing and advanced multi-mode sensors to achieve an improved level of discrimination of scrap from UXOs.”

With prior funding (UX-1225, MM-0437, and MM-0838), LBNL group has successfully designed and built a cart-mounted Berkeley UXO Discriminator (BUD) and demonstrated its performance at various test sites (e.g., Gasperikova et al., 2007, 2008, and 2009).

Hand-held systems have the advantage of being lightweight, compact, portable, and deployable under most site conditions. They are particularly useful in areas of dense vegetation or challenging terrain. In heavily wooded areas or areas with steep or uneven terrain, hand-held sensors may be the only suitable sensor deployment method. A useful criterion might be that it could be carried through spaces that the operator could walk through or at least approach. Further, it is desirable to find and characterize a metallic object without the need to accurately locate the sensors at multiple positions around the target. The ideal system would thus locate and characterize the target from a single position of the sensor and indicate to the operator where to flag the target for subsequent study.

A sensor package of a 14-in (0.35 m) cube was designed and built based on these considerations (UX-1667). This hand-held prototype incorporates the key features of the cart-mounted system – (a) three orthogonal transmitters and ten pairs of receivers, and (b) difference or gradient measurements that significantly reduce the ambient and motion noise, and greatly enhance the sensitivity to the gradients of the target. The system characterizes the target from a single position. Results from a local test site and the Aberdeen Proving Ground (APG) were in a good agreement with theoretical performance calculations of such a device (Gasperikova et al. 2010). This survey was designed to demonstrate the system performance under realistic survey conditions at the former Camp Beale, Marysville, CA.

## 2. TECHNOLOGY DESCRIPTION

The SERDP and ESTCP have supported LBNL in development of a device that not only detects the object itself but also quantitatively determines its size, shape, and orientation. In a hand-held system the sensor package must be easily maneuvered over rough terrain, through brush, etc. A useful criterion might be that it could be carried through spaces that the operator could walk through or at least approach. To avoid the reliance on accurate multiple positioning of any system it has been shown that (1) the object must be illuminated with three different polarizabilities of transmitted field and that (2) to determine location from a single position of the transmitter-receiver system multiple spaced-apart receivers must be used. To accommodate the first requirement a hand-held design implements three orthogonal transmitter loops much like the cart-mounted system. To accommodate the second requirement the hand-held UXO discriminator uses ten pairs of receivers. The same discrimination abilities afforded by the cart-mounted system are available in the hand-held unit albeit with slightly reduced depth of detection. The hand-held UXO discriminator is able to discriminate small (20 mm) objects at a depth of 0.45 m and large (105 and 155 mm) objects at the depth of 0.85 m and detect them down to 1.15 m.

The hand-held UXO discriminator employs three orthogonal transmitters and ten pairs of differenced receivers. Each vertical face of the cube has three induction coils, and two horizontal faces have four induction coils, each sensitive to the magnetic field component normal to the face. Receivers on opposite faces of the cube are paired along the symmetry lines through the center of the system and each pair sees identical fields during the on-time of current pulses in the

transmitter coils. They are wired in opposition to produce zero output during the on-time of the pulses in three orthogonal transmitters. This configuration dramatically reduces noise in measurements by canceling background electromagnetic fields (these fields are uniform over the scale of the receiver array and are consequently nulled by the differencing operation), and by canceling noise contributed by the tilt of the receivers in the Earth's magnetic field, thus greatly enhances receivers' sensitivity to gradients of the target response. The hand-held UXO discriminator (14-in or 0.35 m cube), shown in Figure 1, is able to discriminate small (20 mm) objects at a depth of 0.45 m and large (105 and 155 mm) objects at the depth of 0.85 m and detect them down to 1.15 m. Transmitter-receiver configuration is shown in Figure 2a while the assembled transmitter-receiver cube is shown in Figure 2b.



**Figure 1.** LBNL hand-held UXO discriminator

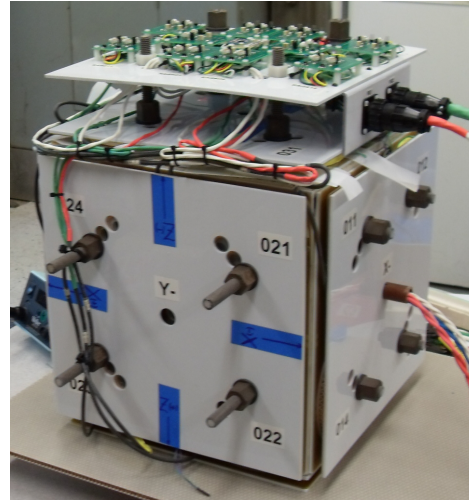
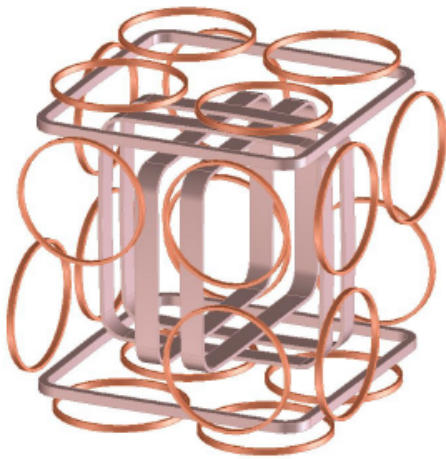


**Figure 2.** LBNL hand-held UXO discriminator: (a) transmitter-receiver configuration, (b) assembled prototype.

Data acquisition is performed on a single board. The transmitter coils are powered separately from the data acquisition board. Pulsers provide resonant circuit switching to create bi-polar half-sine pulses of  $300 \mu\text{s}$  width. The current has a  $\sim 40 \text{ A}$  peak and a resonant circuit voltage of  $\sim 400 \text{ Volts}$ , and the operational overall half-sine duty cycle is  $\sim 12\%$ . Transients are digitized with a sampling interval of  $4 \mu\text{s}$ . The sensors are critically damped 5-inch coils with a self-resonant frequency of  $75 \text{ kHz}$ . The data acquisition board has 12 high-speed ADC channels for output. Ten of these channels are used for the signal from receiver coils, and the remaining two channels provide information about the system (i.e. tilt information, transmitter current).

An important feature of the hand-held UXO discriminator is an inversion algorithm, which is used to determine target properties from measurements with a given transmitter-receiver configuration. At any given time the response is inverted to yield the location (x, y, z) of the target, its attitude and its principal polarizabilities. It has been demonstrated that a satisfactory

classification scheme is one that determines the principal dipole polarizabilities of a target – a near intact UXO displays a single major polarizability coincident with the long axis of the object and two equal transverse polarizabilities. Figures 3 and 4 illustrate a discrimination capability of the system for UXO object and a scrap metal, respectively. While UXO objects have a single major polarizability coincident with the long axis of the object and two equal transverse polarizabilities (Figure 3), scrap metal exhibits three distinct principal polarizabilities (Figure 4). There are clear distinctions between symmetric intact UXO and irregular scrap metal. Moreover, UXO have unique polarizability signatures, and thus distinctions can be made among various UXOs. Object orientation and equivalent dipole polarizability estimates of large and shallow UXO or scrap are more problematic as they are affected by higher order (non-dipole) terms induced in objects due to source field gradients along the length of the objects. In the case of the large and shallow objects, the hand-held system can be easily raised an appropriate distance above the object such that the dipole model approximation for polarizability estimates is appropriate.

UXO and scrap discrimination and priority dig list were done by Signal Innovations Group, Inc. and the approach is described in Chapter 4.2.

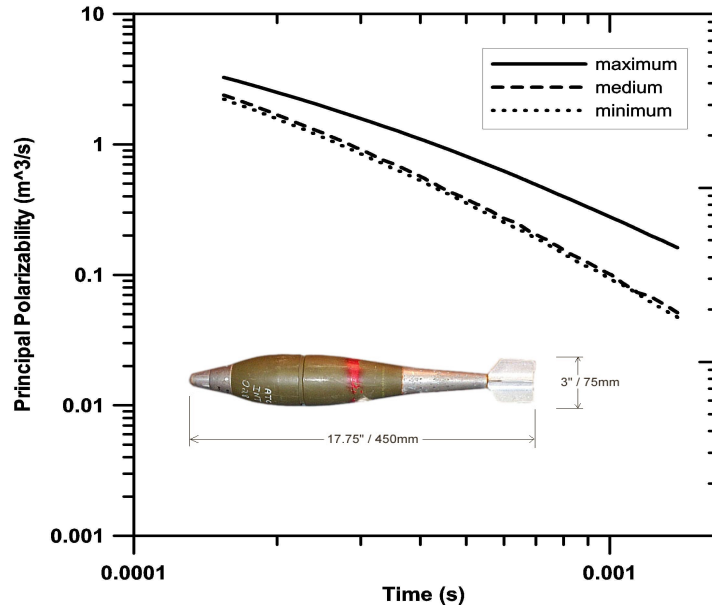


**Figure 3.** Inversion results for the principal polarizabilities of 81 mm mortar.

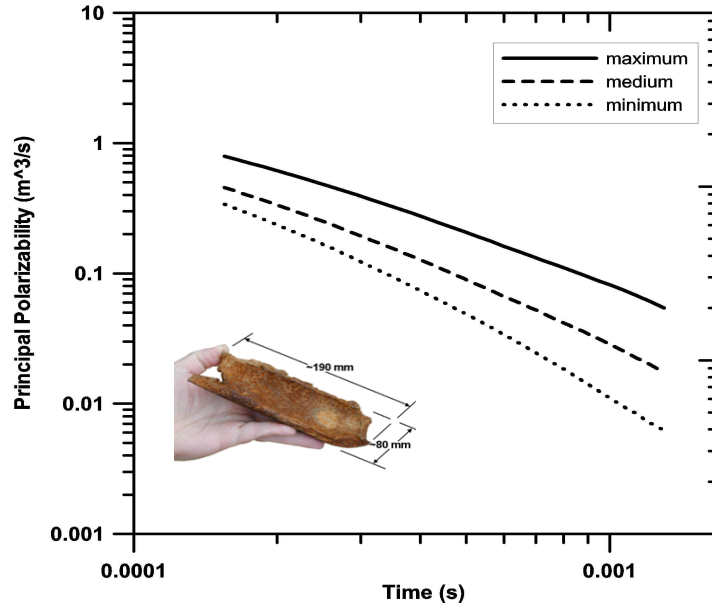


**Figure 4.** Inversion results for the principal polarizabilities of 19x8 cm scrap metal.

### 3. DEMONSTRATION SURVEY

The demonstration survey was performed between June 13 and June 28, 2011. The hand-held UXO discriminator was operated in the cued mode. The system was brought to marked locations (flags) and ran in the characterization/discrimination mode. The three discriminating polarizability responses along with the object depth and horizontal location with respect to the center of the bottom plane of the cube was recorded and visually presented on the computer screen. Additional values recorded with each location were S/N ratio, polarizability index (an average value of the product of time (in seconds) and polarizability rate (in  $m^3/s$ ) over the 46 sample times logarithmically spaced from 80 to 1,460  $\mu s$ ), and the cart orientation, pitch, and roll. Figure 5 illustrates the deployment of the system at the site.



**Figure 5.** LBNL hand-held UXO discriminator at Camp Beale.

Soundings were collected at each flag, and at 0.15 m before and 0.15 m after it, with the system oriented in a single direction. Soundings were differenced with background reference soundings taken within the previous 30-40 minutes at a nearby site determined by the field operator to be free from metallic objects. When polarizability inversions from all three soundings were unrelated to each other, additional two soundings were taken, one on each side of the system, 0.15 m from the flag. The hand-held UXO discriminator surveyed 18 grids that are indicated in Figure 6 in yellow and blue colors. These grids were: J02, J03, J05, J06, K02, K03, K05, K06, R07-09, S02, S03, S07-09, T02, and T03.

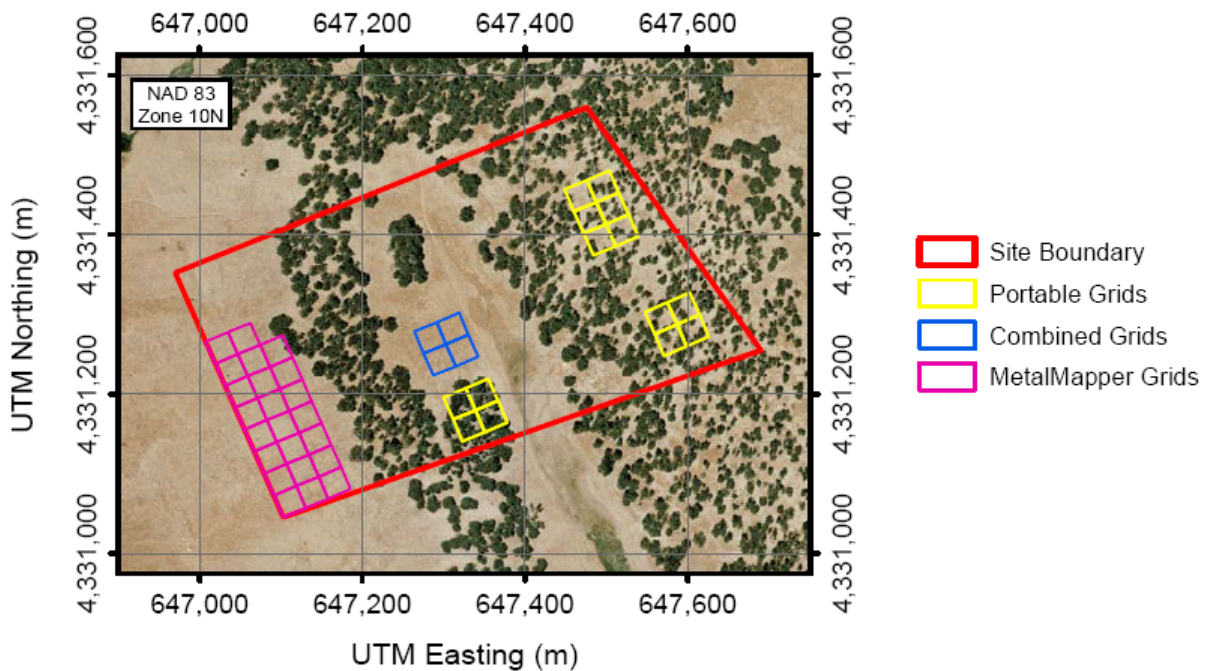


**Figure 6.** Survey area divided into sub-grids.

## **4. DATA ANALYSIS AND INTERPRETATION**

### ***4.1 Data Processing***

Ten channels of field data were recorded at a rate of 250 k-samples/second for each of three transmitters. Field data were stacked together in a field programmable gate array (FPGA) and transferred to a field computer (laptop) forming a primitive stack. An even number of primitive stacks is averaged together to form stacked data for further processing. The peak transmitter current was estimated from the stacked transmitter current channel record, and the data were normalized by that value. Nominal transmitter shut-off time was estimated, and induction responses were computed at 46 logarithmically spaced times between 80 and 1,460  $\mu\text{s}$ , averaged in half-sine windows with widths 10% the center time after transmitter pulse shut-off. Responses were differenced with background responses collected over an area determined to be free of metallic objects. The resulting 30 channels of normalized responses were then inverted for candidate object position and principal polarizabilities as a function of time after transmitter shut-off. These were used as an input for the discrimination approaches described in Chapters 4.2 and 4.3.

### ***4.2 Discrimination Using the Isolate Process***

Signal Innovations Group, Inc. (SIG) applied the Isolate discrimination process in the Camp Beale demonstration. This process involved robust feature extraction and selection and semi-supervised classifier training using active selection of labeled data. As shown in Figure 7, this process was

divided into three main phases: (1) Feature Extraction, (2) Site Learning, and (3) Excavation. Details on each phase are given in the next subsections. The SIG Isolate process leveraged on two feedback steps. The first feedback was in training the semi-supervised classifier, where additional anomaly labels were requested until the classifier reached sufficient stability. The second feedback was during the excavation of anomalies, where the classifier was retrained with additional labeled anomalies until either the UXO/clutter predictions became highly separable or until high probability anomalies were substantially revealed to be clutter upon excavation.

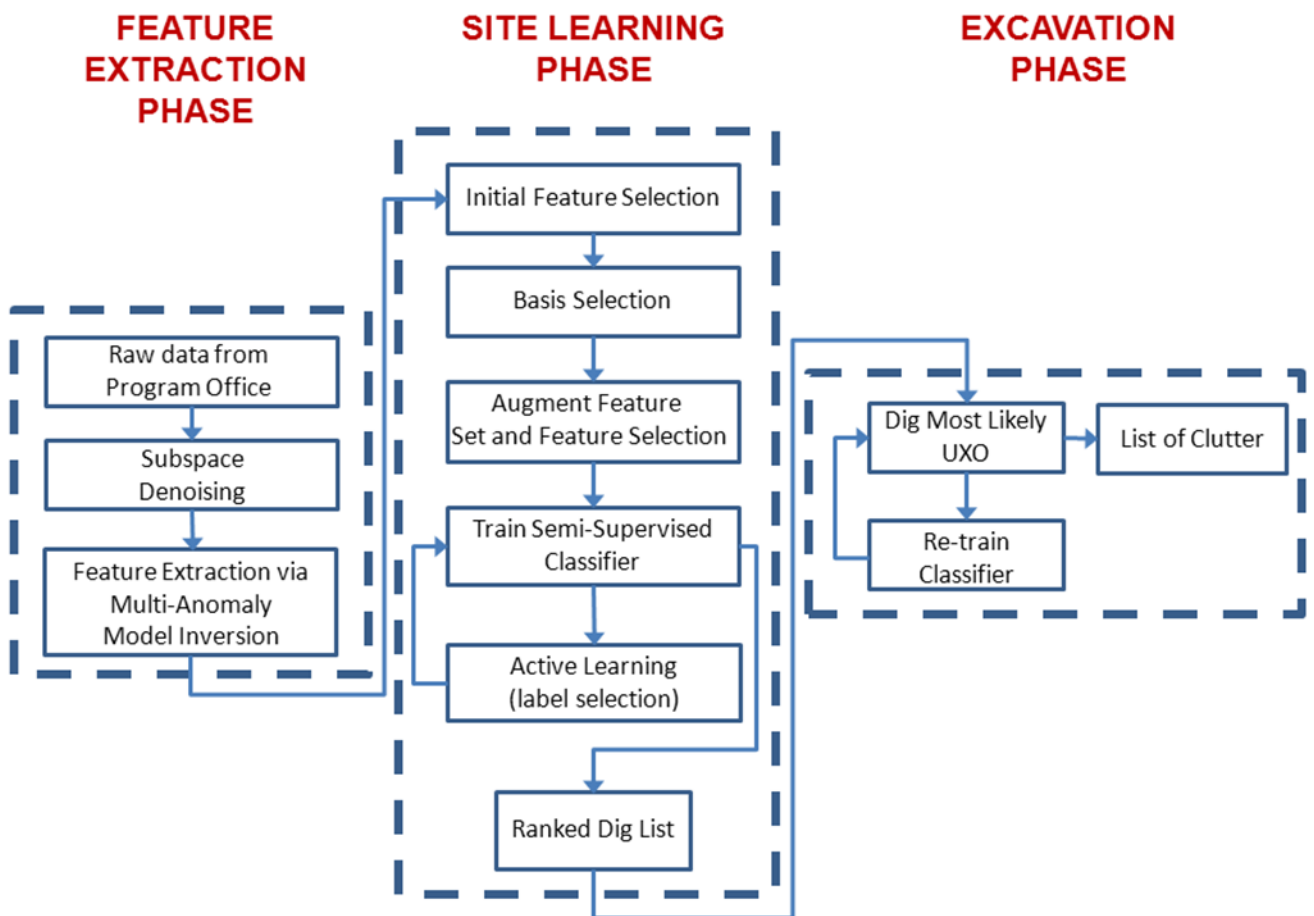


**Figure 7.** Flow diagram of the SIG Isolate process.

### ***4.2.1 Feature Selection with BENet***

Adaptive learning of a classifier *in situ* benefits from refining the appropriate set of extracted features for the targets under test. This occurs because of the ‘curse of dimensionality’ where the number of data points required to cover the breadth of a features space grows exponentially with the number of features considered. If the amount of training data does not sufficiently sample the feature space, then the learned classifier will lack statistical support and class estimate uncertainty is large. Bayesian classification models perform feature selection by placing a sparseness prior on the inferred feature weights. The Bayesian elastic net (BENet) regression model used for feature selection employs a sparseness prior equivalent to a convex combination of L1-norm and L2-norm penalties in a least squares optimization formulation (Zhang et al., 2003; Zhang et al., 2004). The sparseness prior of the BENet model jointly infers the essential subset of relevant features, including correlated features, for a given classification task. Rather than encouraging the selection of a single feature in a set of correlated important features (like similar approaches such as Relevance Vector Machine), the BENet model encourages the selection of all correlated important features. By performing sparse and grouped feature selection, the BENet algorithm provides a more robust approach to feature adaptability and the interpretation of important features, ultimately requiring fewer training data samples to achieve robust statistical support.

### 4.2.2 Semi-Supervised Learning Classifier

Semi-supervised learning is applicable to any sensing problem for which all of the labeled and unlabeled data are available at the same time, and therefore, particularly for the current demonstration study. In most practical applications, semi-supervised learning has been found to yield superior performance relative to widely applied supervised algorithms, which train only on labeled data. The context provided by the unlabeled data is crucial in improving the classification performance especially in cases where the labeled data were not representative of the two class distributions. As the number of training samples increases, the supervised classifier should approximate the semi-supervised classifier. Semi-supervised formulation treats the dataset (labeled and unlabeled) as a set of connected nodes, where the affinity  $w_{ij}$  between any two feature vectors (nodes)  $\mathbf{f}_i$  and  $\mathbf{f}_j$  is defined in terms of a radial basis function (Cristianini and Shawe-Taylor, 2000). Based on the above formulation, one can design a Markov transition matrix  $\mathbf{A} = [a_{ij}]_{N \times N}$  that represents the probability of transitioning from node  $\mathbf{f}_i$  to  $\mathbf{f}_j$ . Assuming  $\mathcal{L} \subseteq \{1, 2, \dots, N_L\}$  represents the set of labeled data indices, the likelihood functional can be written as

$$(\{y_i, i \in \mathcal{L}\} | \mathcal{N}(\mathbf{f}_i), \boldsymbol{\theta}) = \prod_{i \in \mathcal{L}} p(y_i | \mathcal{N}(\mathbf{f}_i), \boldsymbol{\theta}) = \prod_{i \in \mathcal{L}} \sum_{j=1}^{N_i} a_{ij} p(y_i | \mathbf{f}_j, \boldsymbol{\theta})$$

where  $\mathcal{N}(\mathbf{f})$  defines the neighborhood of  $\mathbf{f}$ . Estimation of classifier parameters  $\boldsymbol{\theta}$  can be achieved by maximizing the log-likelihood via an Expectation-Maximization algorithm (Liao and Carin, 2008). To enforce sparseness of  $\boldsymbol{\theta}$  (enforcing most of the components of the parameter vector  $\boldsymbol{\theta}$  to be zero), one may impose a zero-mean Gaussian prior on  $\boldsymbol{\theta}$ . A zero-mean

Gaussian prior with appropriate variance can strongly bias the algorithm in choosing parameter weights that are most likely very small (close to zero).

### 4.2.3 *Batch-mode Active Learning (AL)*

Given that available training data labels at the beginning of a demonstration are not available and that excavations must be performed to reveal training data labels, one may ask in which order anomalies should be excavated to maximally improve the performance of the classifier algorithm. One useful criterion is to use the confidence on the estimated identity of the anomalies that are yet to be excavated. Specifically, one may ask which unlabeled anomaly label would be most informative to improve classifier performance if the associated label could be made available. It has been shown by MacKay (1992) that this question can be answered in a quantitative information-theoretic manner.

For active label selection, posterior distribution of the classifier is approximated as a Gaussian distribution centered on the maximum a posteriori (MAP) estimate. The uncertainty of the classifier is quantified in terms of the posterior precision matrix. The objective of AL is to choose a feature vector for labeling that maximizes the mutual information ( $I$ ) between the classifier  $\theta$  and the new data point to be labeled. The mutual information can be quantified as the expected decrease of the entropy of  $\theta$  after new sample  $\mathbf{f}_{i^*}$  and its label  $y_{i^*}$  are observed.

$$I = \frac{1}{2} \log \frac{|H'|}{|H|} = \frac{1}{2} \log \{1 + p(y_{i^*} | \mathbf{f}_{i^*}, \theta) \times [1 - p(y_{i^*} | \mathbf{f}_{i^*}, \theta)] \mathbf{f}_{i^*}^T H^{-1} \mathbf{f}_{i^*}\}$$

It is important to note that the mutual information  $I$  is large when  $p(y_{i^*} | \mathbf{x}_{i^*}, \theta) \approx 0.5$ . Hence, the AL prefers to acquire labels on those unlabeled samples for which the current classifier is most

confused or uncertain. In this fashion the classifier learns quickly by not excavating anomalies that reveal redundant information. The process continues as new labels are revealed until the expected information gain for the remaining anomalies is approximately uniformly low. At that point the classifier is adequately trained and target inference on the remaining unlabeled anomalies can be reliably performed. By invoking the principle of submodularity in the algorithm optimization, the approach has been adapted to allow for the selection of multiple simultaneous labels at one time, making the technique operationally practical.

#### 4.2.4 SIG Isolate Process Overview

The SIG Isolate process can be summarized in the following steps (Figure 7):

- **Data Conditioning** - First, raw, unlabeled anomaly data are received.
- **Subspace Denoising** - The anomaly data are denoised to ensure robust performance for discriminating late time-gate features.
- **Feature Extraction** - A robust multi-anomaly dipole model is fitted to the data. The polarizability parameters from this fitting become the set from which features are drawn for classifier training. In addition to the time-domain polarizabilities, a set of 9 ‘rate’ features were calculated. These features were calculated by fitting the time-domain polarizabilities of each axis to an exponential-decay model:

$$p_i = r_{1i} + r_{2i}e^{\frac{-t}{r_{3i}}}$$

where  $i \in \{x, y, z\}$  is the current axis,  $p$  is the polarizability,  $t$  is time and  $\{r_1, r_2, r_3\}$  are the fitted rate parameters. The optimized values of the rate parameters were found using non-linear least squares.

- **Basis Selection** - A few of the many possible features are selected based on their physical interpretation as they relate to the anomaly, and, using these features, the most informative set of anomalies are selected via an information metric to begin classifier training.
- **Feature Set Augmentation** - The feature set is then augmented by adding early, mid and late time polarizabilities values.
- **Automated Features Selection** - The most relevant set of features is selected from the larger feature set using BENet.
- **Semi-supervised Parametric Neighborhood-Based Classifier (PNBC) Training (STL or MTL)** - When the PNBC is trained only using data from the current site of interest, it is called Single Task Learning (STL). When the PNBC is trained for multiple sites simultaneously it is called MTL.
- **Batch-mode Active Learning** - Based on the estimates made with the PNBC classifier, a new set of anomalies are selected for labeling using batch-mode AL. The goal at this step is to maximize the information gain from new labels requested from the set of unlabeled anomalies. The process is repeated as the PNBC classifier adequately learns data manifold. The stopping criterion for the learning process is apparent when the remaining unlabeled data points have approximately equal information for improving the classifier, and labeling any one anomaly is no better than any other.
- **Excavation Adapted Threshold Selection** - At this point, the highest probability UXO are selected for excavation and labels. The classifier continues to be retrained when new labels are revealed. This process continues until the highest probability UXO items excavated are all found to be clutter at which point digging stops.

#### 4.2.5 Application to Camp Beale Data

The feature extraction phase started with selecting anomaly responses for the analysis. As described in Chapter 3, three or five measurements were made around the flag, and polarizability responses obtained by a single dipole inversion performed during field data acquisition were used. We developed two methods for selecting a single template position to represent the anomaly. The first method selected the template position where the anomaly was estimated to be closest to the sensor, hereafter referred to as the ‘closest’ method. That is, the inversion estimate of the horizontal distance from the anomaly to the sensor was smallest. If the flag location were correct, we expected the central template position (#2), to be selected most frequently. However, our results showed that template positions #1 and #4 were selected more frequently than the template position #2 (Figure 8b). This suggests that the flag locations relative to the anomaly were frequently outside the range of a single sensor sounding. The second method was to select the template position whose anomaly was most symmetric along the transverse axes, hereafter referred to as the ‘symmetric’ method. We calculated symmetry using the mean squared difference between log polarizabilities for the 2<sup>nd</sup> and 3<sup>rd</sup> axes:

$$S_i = \sqrt{\frac{\sum_{t=1}^T (p_{i,y,t} - p_{i,z,t})^2}{T}}$$

where  $i \in \{1, \dots, 5\}$  is the template position,  $p$  is the log polarizability at time  $t \in \{1, \dots, T\}$  for the transverse axes  $y$  and  $z$  (Figure 8a).

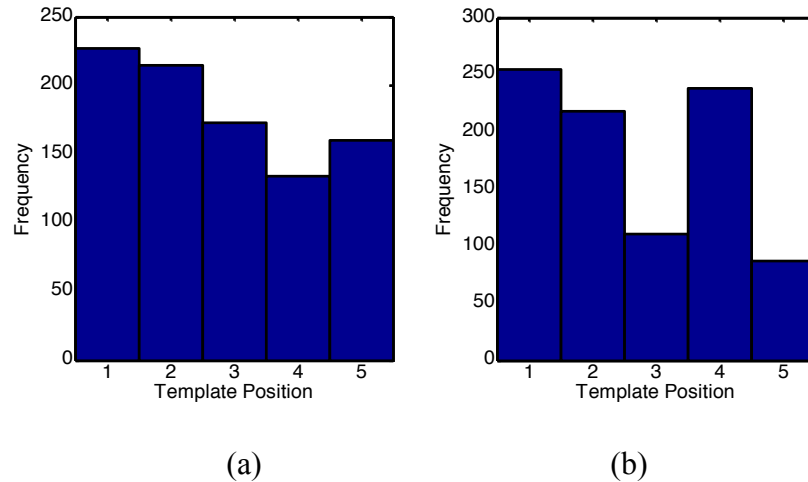


**Figure 8.** Histogram of the selected template position for the sensor across all anomalies in BealeTrees for the (a) ‘symmetric’ and (b) ‘closest’ methods. Template position #2 is the central template position.

Having selected a single template position for each flag using these two methods, training began by selecting an initial basis of 30 vectors maximizing Fisher Information Gain. This initial selection was the same for both the ‘closest’ and ‘symmetric’ methods. From this initial sample a set of relevant features was selected using BENet, and a non-linear PNBC classifier trained on these features. Then, a new set of 10 unlabeled anomalies were selected using batch AL. The labels for these anomalies were requested and the training process was repeated until new labels did not provide a substantial amount of new information. The total number of training rounds for the ‘closest’ was 11 and the total number for the ‘symmetric’ method was 10 (Figure 9). At the end of training there were many more features that were relevant for discrimination in the ‘closest’ method than the ‘symmetric’ method. This is likely due to the fact that the ‘closest’ method selected the wrong template position to represent an anomaly more frequently than the ‘symmetric’ method did.

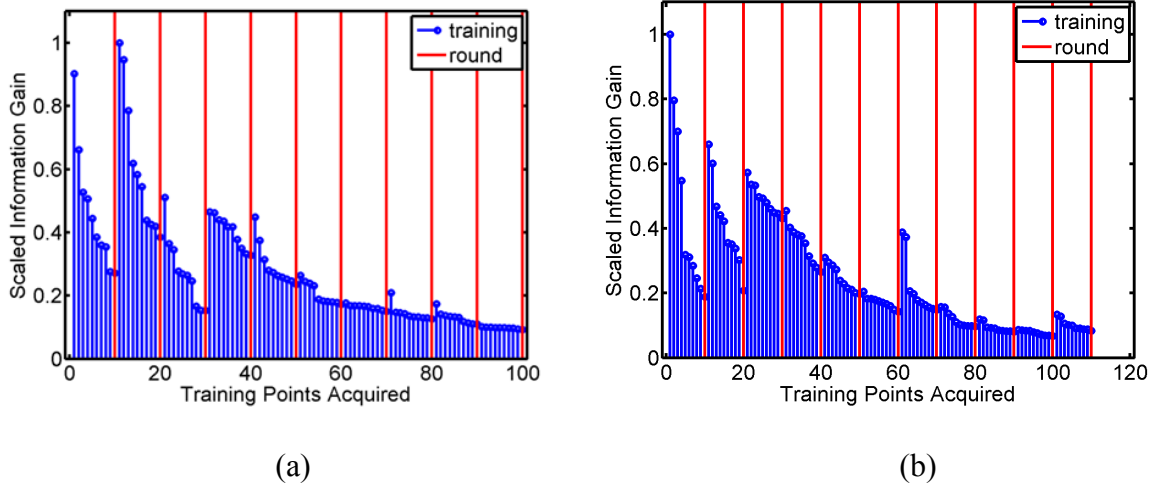


**Figure 9.** Fisher Information Gain through all training rounds for the (a) 'symmetric' and (b) 'closest' methods.

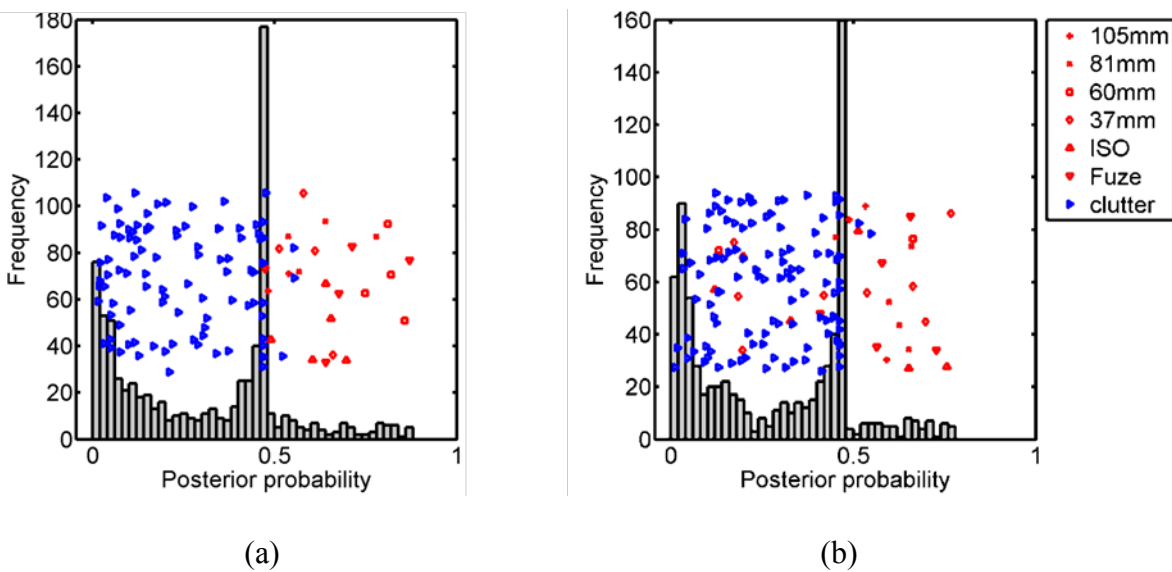


**Figure 10.** Distribution of posteriors for the (a) 'symmetric' and (b) 'closest' methods at the end of training.

At the end of training the posterior probabilities of unlabeled samples (Figure 10) showed that the 'closest' method was not as separable as the 'symmetric' method at this stage; some predicted probabilities for the previously labeled UXO were less than 0.5. We dug unlabeled observations, beginning from the highest posterior probability, and proceeded until we had dug a

total of 30% of the site (including training data). There were three ‘can’t analyze’ anomalies, whose positions were too far from the sensor to be reliable (BE-0609, BE-0879, and BE-0887). After receiving the labels (ground truth) for this first round we missed eight seeds in the ‘closest’ method and three seeds in the ‘symmetric’ method. Given these missed seeds we retrained and requested 43 additional labels for the ‘closest’ method, and eight additional labels for the ‘symmetric’ method. After receiving those labels, we decided to stop digging the ‘closest’ method, but continued digging the ‘symmetric’ method by requesting eight, then 28, and finally 22 additional labels. The total number of ranked anomalies (those dug but not counted in the training or ‘can’t analyze’ sets) at the end of digging was 208 for the ‘symmetric’ method and 184 for the ‘closest’ method. The decision to stop digging the ‘closest’ method was made because our last 50 digs were clutter, even though there still remained 20 anomalies with a posterior probability greater than 0.5 (Figure 11). In retrospect, digging these remaining anomalies would not have revealed any target of interest (TOI).

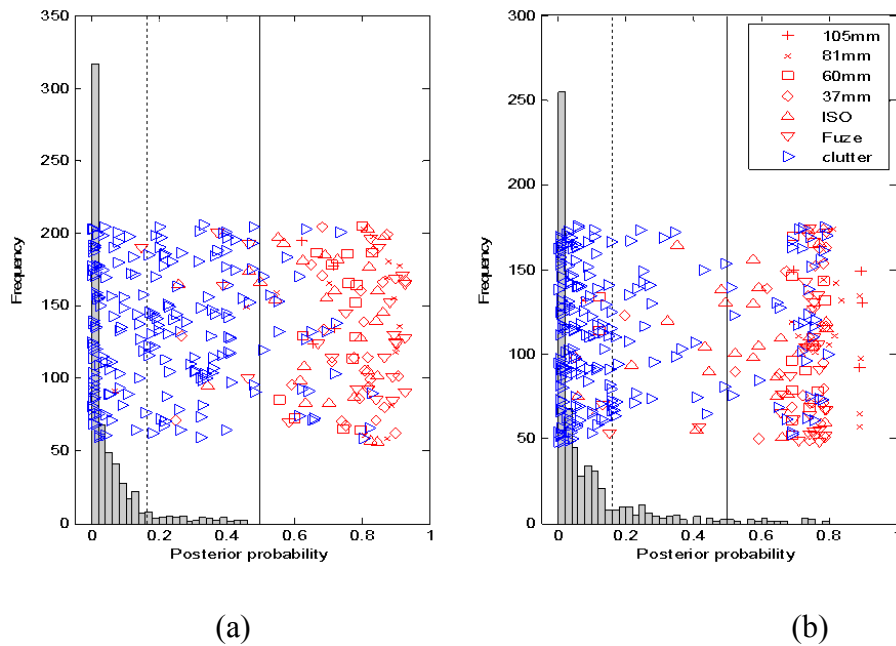


**Figure 11.** Posteriors distributions at the end of digging for the (a) 'symmetric' and (b) 'closest' methods.

#### ***4.2.6 Retrospective Analysis***

We missed a group of fuzes that are fairly similar in a feature space. The primary reason we missed this type of targets lies in our feature selection process. Each time a classifier was built, the feature space was pruned to only those features that were linearly discriminative of UXO and clutter. But, the set of features that was discriminative for most of the UXO was not the same set of features that was discriminative for fuzes (Figure 12). A solution to this problem would be to create a separate classification for fuzes. A secondary reason for missing these fuzes was that they were surrounded by clutter in the feature space. Figure 13 shows that while the missed fuzes are clustered along the primary axes of feature variation, there are also many clutter items close to them. During active learning we received labels for anomalies close to this cluster of fuzes, and they were all clutter. So, any model we fit to those labels would assign a low probability of being UXO to the fuzes. Again, this could be remedied by using features that were uniquely discriminative for fuzes rather than being discriminative of the entire dataset (as in Figure 13) or all UXO combined (as in our BENet feature selection).

In terms of selection algorithm performance, the ‘symmetric’ algorithm tended to have fewer incorrectly selected template positions than the ‘closest’ method. There are a few lines of evidence for this. The first is based on the variance of features for UXO, which was lower for the ‘symmetric’ method than the ‘closest’ method.

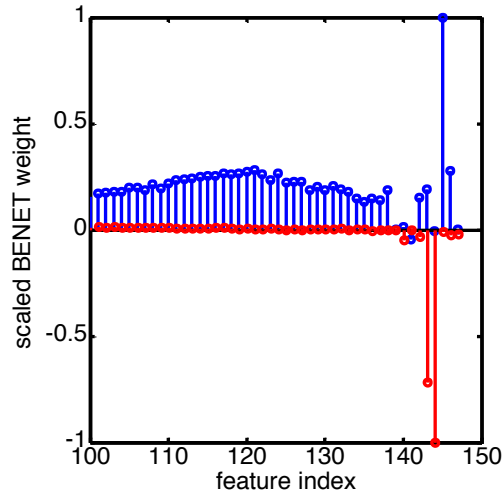


**Figure 12.** Feature weights from BENet on all labeled anomalies for all UXO (blue) and fuzes only (red).

The second line of evidence for the ineffectiveness of the ‘closest’ method is the spread of UXO in the two-dimensional ordination for the ‘closest’ method (Figure 13). There are noticeable UXO outliers in the dominant feature axes suggesting the polarizability responses for these UXO are substantially different from the mean responses of UXO. These outliers are not present in the ‘symmetric’ method, leading us to believe these outliers are the result of selecting an incorrect template position in the ‘closest’ method. An example of inappropriate selection is shown in Figure 14. For this ISO every other template position had an ‘UXO-like’ response except the one chosen by the ‘closest’ method. The reason for such inappropriate selection is straight-forward. There is a piece of clutter underneath template position #4; one not associated with the flagged anomaly. This piece of clutter is closer to the sensor than the UXO was to any of the other template positions, so the ‘closest’ method selected it.

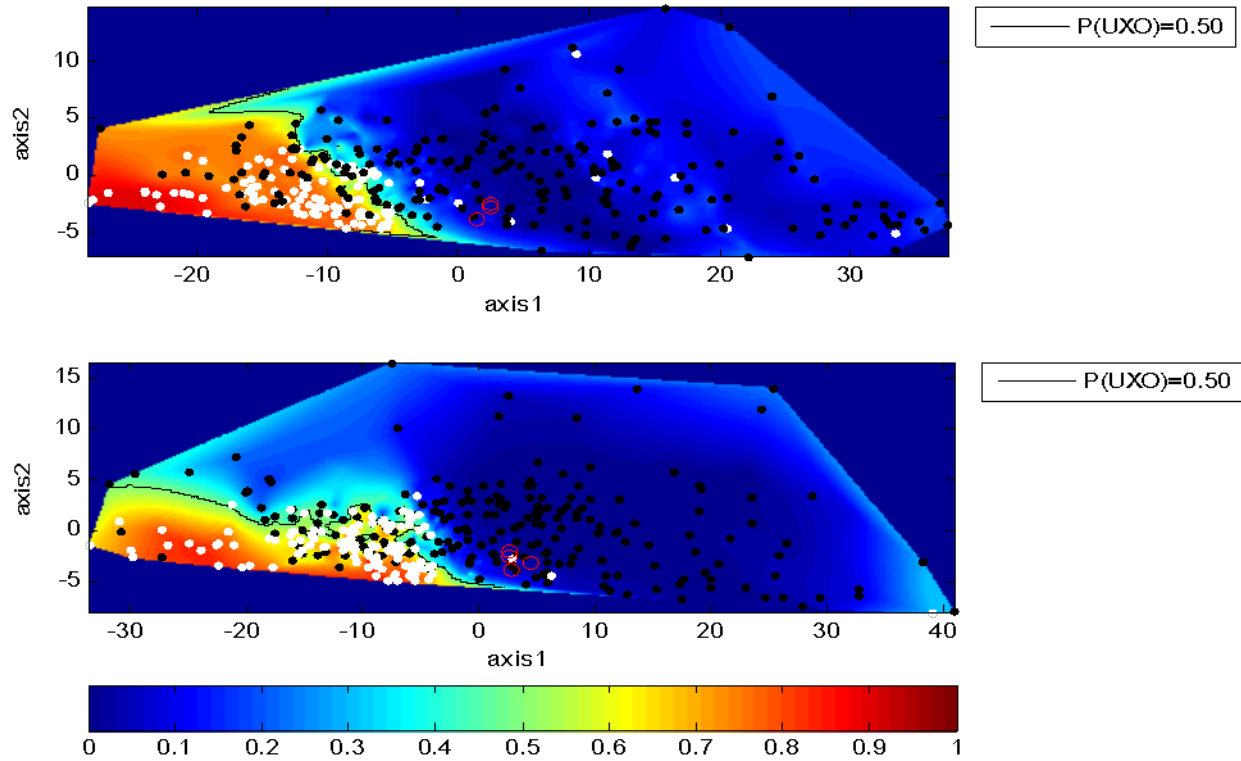


**Figure 13.** MAP estimates (color scale) along two-dimensions of a non-linear ordination of the anomaly features for the ‘closest’ method (top) and the ‘symmetric’ method (bottom). The anomalies that were marked as ‘dig’ in our dig list are shown (UXO in white, clutter in black). The missed fuzes for each method are shown by red circles.

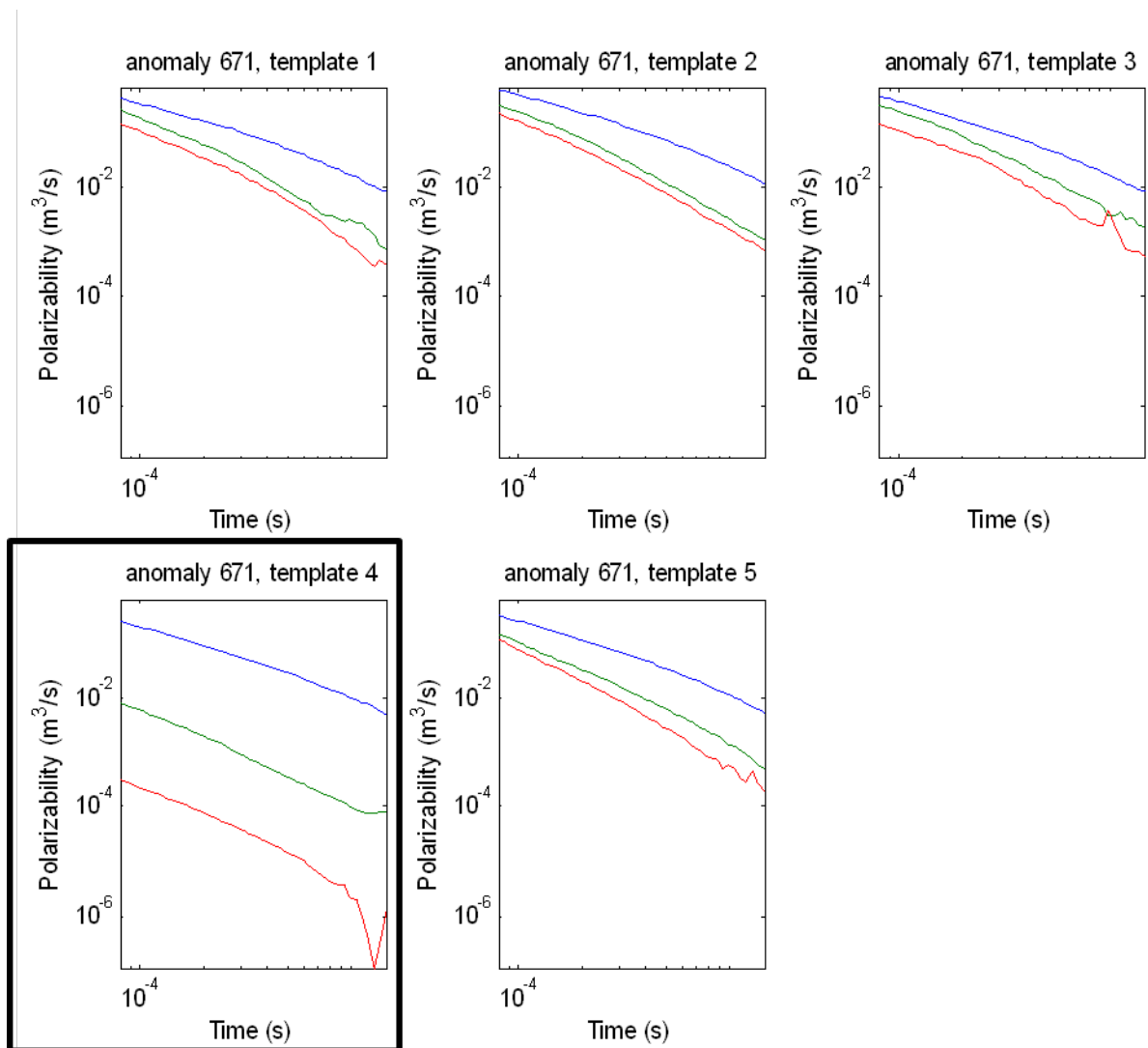


**Figure 14.** Polarizabilities for flag BE-0671, which is an ISO. The 'closest' method selected template position #4 (black box), while all other responses are more UXO-like.

### 4.3 Discrimination Using Template-match Approach

#### 4.3.1 Data Analysis

As described in Chapter 3, data were collected using the three or five-point template placed at the flag location. The orientation of the system was based on the ease of access and the hill slope. Data in J and K grids were collected with the system oriented towards NW (310-320°), in R7-9 and S7-9 grids towards SSE (140-170°), and S2-3 and T2-3 towards SSW (190-210°) (Figure 15a). The hill slope, or tilt of the system, varied up to 15-20° (Figure 15b).

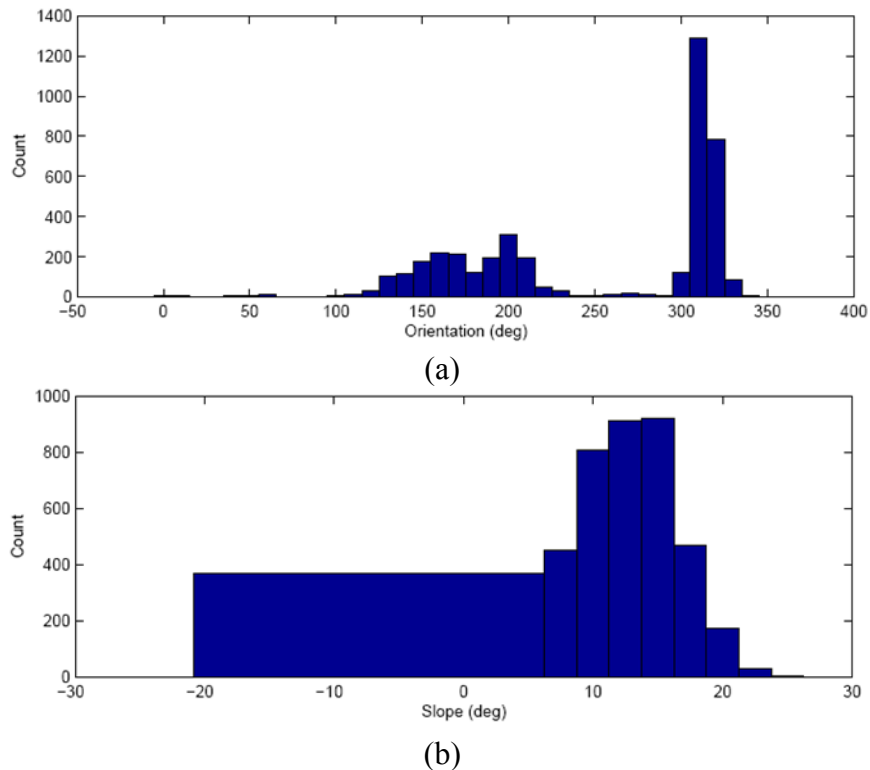


**Figure 15.** Histogram of (a) system orientation, and (b) slope during the survey.

For the discrimination we selected one representative response per flag, based on the polarizabilities magnitude and symmetry, to ensure that if multiple objects were near the flag the response of the most dangerous item would be selected. Figure 16 shows that the distribution

was more or less even among four template positions. The template position #4 was selected less frequently since it was uphill from the flag and therefore further away from the object. Only about 20% of the flags had three measurements, thus we analyzed more than 4,000 measurements.

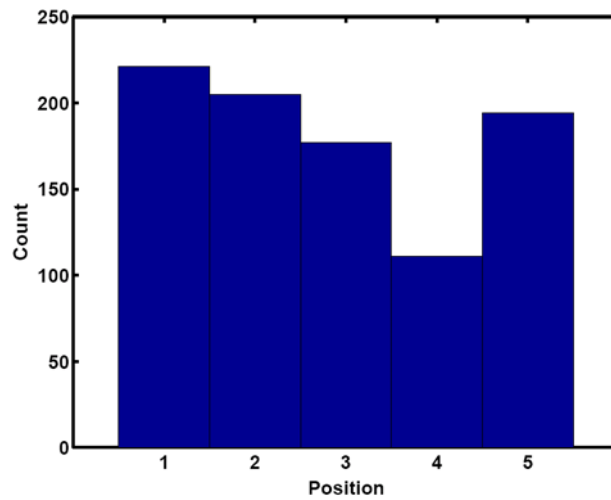


**Figure 16.** Histogram of the selected template position for the responses used in discrimination. Position #2 is the central template position.

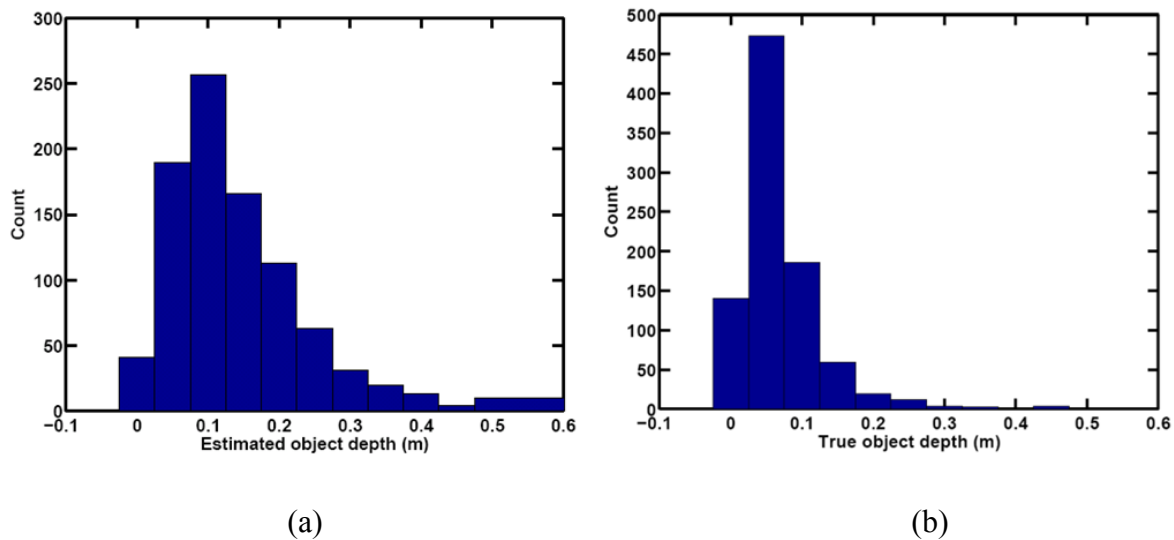


**Figure 17.** Histogram of (a) estimated and (b) true object depths.

Figure 17 shows a very good agreement between objects depths estimated by inversion (a) and true objects depths (b), and that less than 5% of the objects were deeper than 0.3 m.

While running multiple objects inversions takes a long time and therefore it is impractical in the field, single object inversions are very fast and available right after the data are acquired. Therefore we have been developing and evaluating a discrimination approach that could be used in a near-real time in the field. This template-match approach used data processed in the field using a single object inversion, and compared polarizability curves of unknown objects to the polarizabilities of the representative objects in the library. Any single object with a polarizability index value larger than 50% of that of 37-mm projectile (smallest UXO) was considered as a potential object of interest. Parameters used in this approach were (a) the similarity of major polarizability curves, (b) the similarity of medium and minor polarizability curves, (c) the polarizability index, and (d) the flag's average polarizability index. We used data from 100 flags for training, which was about 12% of the whole dataset. Training data were used to verify whether single object inversions could be used for discrimination, and to determine the operating point at which is safe to stop digging. The ranked anomaly list that had the operating point set at 486 is discussed in Chapter 5, and the retrospective analysis is provided in Chapter 4.3.2.

#### ***4.3.2 Retrospective Analysis***

Due to a slight misunderstanding what was considered as TOI, our original stop-digging point was too conservative. If small fuzes were not considered as TOI, we could have stopped much sooner and saved additional 150 digs. Additional savings could be achieved if digging would be

done by contiguous grids. This digging approach, however, needs a follow-up analysis, since only data from one contiguous area or previously excavated areas could be used for training, which wasn't done in the presented approach. Our training data selection and distribution among survey grids suggests that this is feasible.

The last UXO on the ranked anomaly list was 81-mm mortar (BE-4). Given the object size and depth, the measured response wasn't representative of this object, and this location should have been classified as 'can't analyze'. Doing so would save 50 clutter digs.

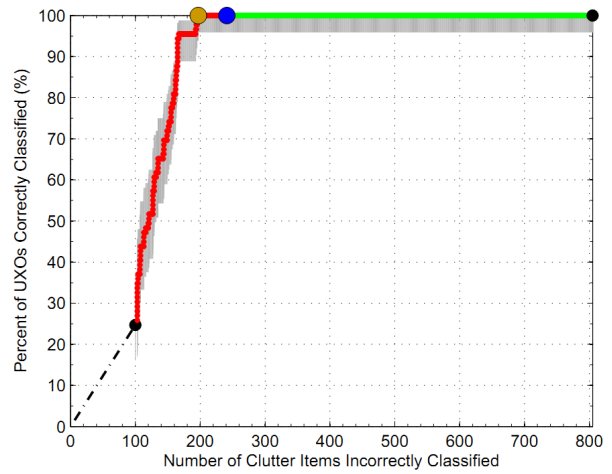
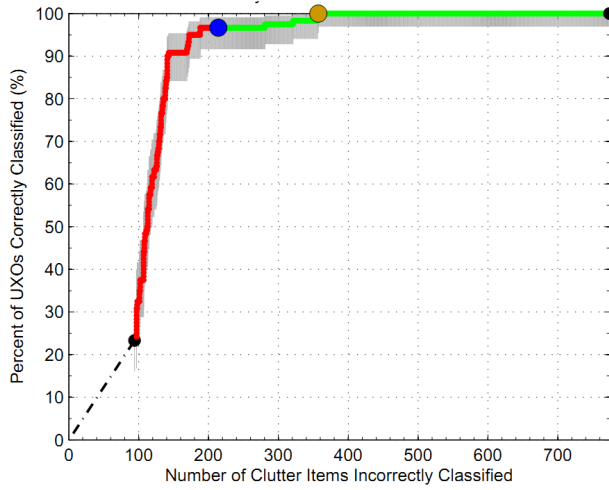
Two types of fuzes were present at the site – (a) 60-mm fuzes that had the polarizability index comparable with the response of 37-mm projectile and were correctly identified using our original approach, and (b) 50-mm fuzes, which responses were much smaller and we missed two of them using the same approach. If this approach would be used for real-time discrimination in the field, and these small fuzes would be considered as TOIs, we could include their response to our library of representative responses, and redefine criteria for setting up the operating point at two different stages – (a) after training data or (b) after digging the highest ranked anomalies reveal such item. Our training data contained small fuzes, however, they were from flags with multiple objects. In this case, we would have to either acquire data over the pit or run a multi-object inversion to obtain a single fuze polarizability response. Even if acquiring data over the pit wouldn't be possible, and we did not include it to the library during the training data stage, our ranked anomaly list had the remaining three single small fuzes at positions 18, 201 and 226. Thus we would encounter them before our stop-digging point, and at this point it would be still feasible to include the response to the library and regenerate the ranked anomaly list.

## 5. PERFORMANCE ASSESSMENT

For the hand-held prototype performance evaluation we submitted a separate ranked anomaly list for each of the approaches described in Chapter 4. Each flag was assigned the rank, category, and dig/no-dig decision. The lowest rank had the flags which either ‘can’t be analyzed’ or had the high probability of being of UXO, then those labeled as ‘can’t decide’, and the highest rank had flags that had a high probability of being scrap. The category was either training data, or test data, and dig/no-dig decision had values either one or zero. All locations with dig equal to one were dug.

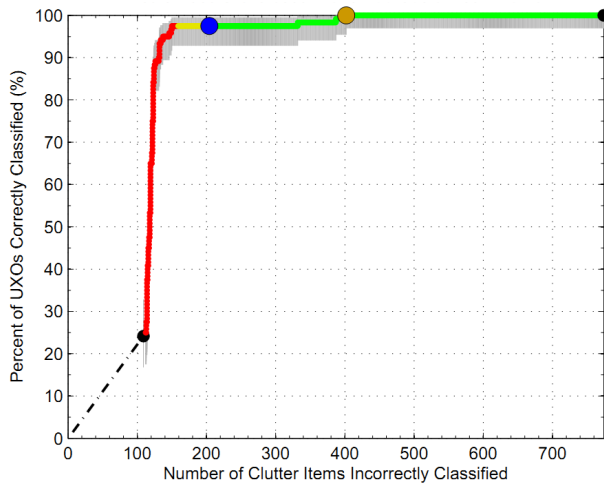
### *5.1 Statistical Approach Performance*

Both the ‘symmetric’ and ‘closest’ methods ended digging up all the TOI when fuzes were considered clutter (Figure 18). The ‘closest’ method performed better than the ‘symmetric’ method in number of false alarms to reach the last UXO: 180 vs. 200. We would consider both methods to be conservative given the fact that we dug approximately 50 extra clutter items after all the non-fuze TOI had been revealed, and given that we acquired over 100 training labels using AL in both methods. In theory this means that we thoroughly explored the feature space for hidden modes of TOI. But, the ‘closest’ method missed three fuzes and the ‘symmetric’ method missed four fuzes when these items were considered TOI. Both methods missed BE-0482, BE-558, and BE-0805, and the ‘symmetric’ method additionally missed BE-0697. The reasons why we missed these fuzes are given in Chapter 4.2.6.

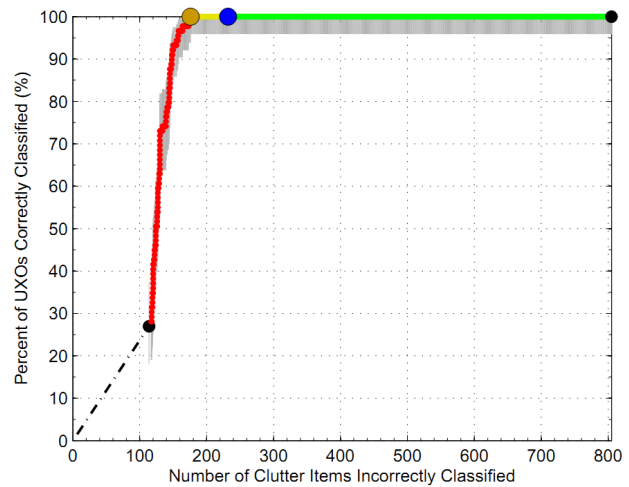


(a)

(b)



(c)



(d)

**Figure 18.** ROC curves for the 'symmetric' method (top) and the 'closest' method (bottom). Fuzes are treated as UXO (left) and clutter (right).

## 5.2 Template-match Approach Performance

The template-match approach used the criteria described in Chapter 4.3 to select the operating point (dig threshold), and Figure 19 illustrates that even with those criteria more than 40% of anomalies were correctly labeled as non-dangerous if the smallest fuzes were not considered as TOIs. This operating point (blue dot) was very conservative, and the retrospective best dig threshold (yellow dot) would save another 150 digs. If the anomalies would be excavated grid-by-grid, additional 80 holes would be saved (magenta dot). We missed two small fuzes (BE-558 and BE-0805), if they were considered as TOIs. Our retrospective analysis in Chapter 4.3.2 describes possible solutions, and suggests that this approach could potentially save more than 60% of clutter digs if the operating point would be selected iteratively based on the information from digging locations that were high on the ranked anomaly list.

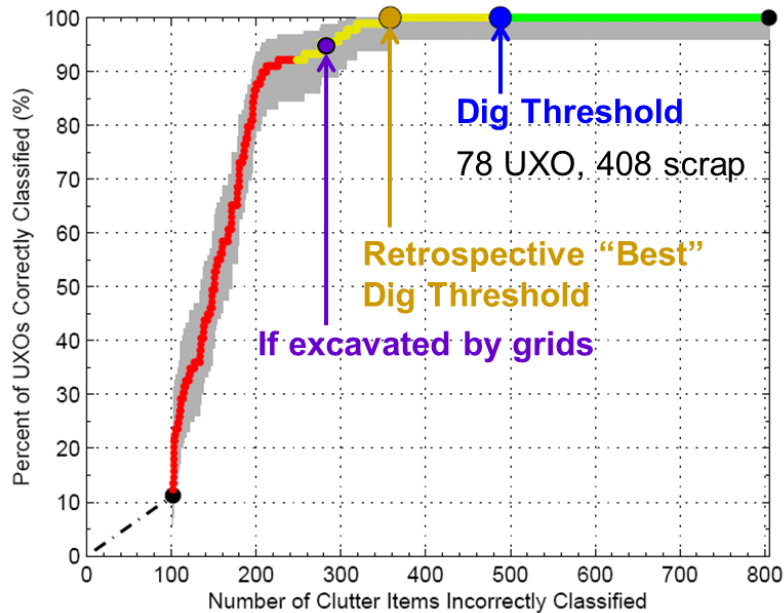


**Figure 19.** The template-match approach ROC curve. Fuzes are treated as clutter.

## **6. CONCLUSIONS**

This survey showed that the same discrimination capabilities afforded by the cart-mounted system are available in the hand-held unit, although with a slightly reduced depth of detection. The survey in a steep terrain in wooded areas was challenging but feasible. While the system is operable by a single operator, because it has no positioning navigation, the second person was necessary to ensure the system was positioned correctly at the template positions. We had no downtime, collected over 4,000 measurements, and finished the survey in two weeks. The discrimination results were excellent – only 25% of the anomalies had to be excavated to find every TOI. Moreover, our near-real time discrimination approach also showed promising results.

## **7. ACKNOWLEDGMENTS**

This work was partially supported by the U.S. Department of Energy and LBNL under Contract No. DE-AC02-05CH11231, and the U. S. Department of Defense under the Environmental Security Technology Certification Program Project MR-201166. Funding for Signal Innovations, Inc. was provided by the Strategic Environmental Research and Development Program Project MR-1708.

## 8. REFERENCES

Baum, D., L. Doolittle, R. Lafever, M. Monroy, E. Norum, M. Placidi, A. Ratti, C. Serrano, V. Vytla, H. Yaver, 2010, BUD Hand Held, Technical Specification and System Design, LBNL Engineering Report.

Cristianini, N. and J. Shawe-Taylor, 2000, An Introduction to Support Vector Machines and other kernel-based learning methods. Cambridge University Press.

Gasperikova, E., Vytla, V., Jobe, T., Kennedy, L., and Zhu, X., 2011, Cued survey with a hand-held UXO discriminator at Camp Beale, Partners in Environmental Technology Technical Symposium & Workshop, Washington D.C.

Gasperikova, E., Smith, J.T., Kappler, K., Morrison, H.F., and Becker, A., 2010, Hand-held UXO Discriminator, SERDP Report.

Gasperikova, E., K.N. Kappler, J. T. Smith, H.F. Morrison, and A. Becker, 2010, Hand-held UXO discriminator design and performance, Partners in Environmental Technology Technical Symposium & Workshop, Washington D.C.

Gasperikova, E., Smith, J.T., Morrison, H.F., Becker, A., and Kappler, K., 2009, UXO detection and identification based on intrinsic target polarizabilities – A case history: *Geophysics*, 74, B1-B8.

Gasperikova, E., J. T. Smith, H. F. Morrison, A. Becker, 2008, UXO Identification Using Berkeley UXO Discriminator (BUD), IEEE International Geoscience & Remote Sensing Symposium, Boston, MA

Gasperikova, E., Smith, J.T., Morrison, H.F., Becker, A., 2007, Berkeley UXO Discriminator (BUD): SAGEEP, Denver.

Gasperikova, E., J. T. Smith, H. F. Morrison, A. Becker, 2007, UXO Detection and Discrimination with Berkeley UXO Discriminator (BUD), UXO Forum, Orlando, FL

Gasperikova, E., J. T. Smith, H. F. Morrison, A. Becker, 2007, Berkeley UXO Discriminator (BUD) at Camp Sibert, AL, Partners in Environmental Technology Technical Symposium & Workshop, Washington D.C.

Gasperikova, E., J. T. Smith, H. F. Morrison, A. Becker, 2007, BUD Results from ESTCP Demonstration Sites, Partners in Environmental Technology Technical Symposium & Workshop, Washington D.C.

Liao, X. and L. Carin, 2008, Migratory Logistic Regression for Learning Concept Drift Between Two Data Sets With Application to UXO Sensing: IEEE Transactions on Geoscience and Remote Sensing, 46, 1454-1466.

MacKay, D., 1992, Information-based objective functions for active data selection: Neural Computation, 4, 589–603.

Smith, J.T., Morrison, H.F., and Becker, A., 2005, Optimizing receiver configurations for resolution of equivalent dipole polarizabilities in situ: IEEE Trans. Geosci. Remote Sensing, 43, 1490-1498.

Zhang, Y., H.Y.L. Collins, C. Baum, and L. Carin, 2003, Sensing of unexploded ordnance with magnetometer and induction data: Theory and signal processing: IEEE Transactions on Geoscience and Remote Sensing, 41, 1005–1015.

Zhang, Y., X. Liao, and L. Carin, 2004, Detection of buried targets via active selection of labeled data: application to sensing subsurface UXO: IEEE Transactions on Geoscience and Remote Sensing, 42, 2535–2543.

## 9. ACRONYMS

AL	Active Learning
BENet	Bayesian Elastic Net
BUD	Berkeley UXO Discriminator
ESTCP	Environmental Security Technology Certification Program
FPGA	Field Programmable Gate Array
IDA	Institute for Defense Analyses
LBNL	Lawrence Berkeley National Laboratory
MAP	Maximum <i>a posteriori</i>
MTL	Multi-task learning
PNBC	Parametric Neighborhood-Based Classifier
ROC	Receiver Operating Characteristic
SERDP	Strategic Environmental Research and Development Program
SIG	Signal Innovations Group, Inc.
S/N	Signal-to-noise
TOI	Target of Interest
UXO	Unexploded Ordnance